Northumbria Research Link

University**Library**

Journal of
Materials Chemistry A

Accepted Manuscript

Journal of
Materials Chemistry A

Materials for energy and sustainability
www.rsc.org/MaterialsA

Volume 4 | Number 1 | 7 January 2016 | Pages 1–330

ISSN 2050-7488

ROYAL SOCIETY OF CHEMISTRY

PAPER
Kun Chang, Zhaorong Chang et al.
Bubble-template-assisted synthesis of hollow fullerene-like
MoS₂ nanocages as a lithium ion battery anode material

175 YEARS

This is an Accepted Manuscript, which has been through the Royal Society of Chemistry peer review process and has been accepted for publication.

Accepted Manuscripts are published online shortly after acceptance, before technical editing, formatting and proof reading. Using this free service, authors can make their results available to the community, in citable form, before we publish the edited article. We will replace this Accepted Manuscript with the edited and formatted Advance Article as soon as it is available.

You can find more information about Accepted Manuscripts in the author guidelines.

Please note that technical editing may introduce minor changes to the text and/or graphics, which may alter content. The journal's standard Terms & Conditions and the ethical guidelines, outlined in our author and reviewer resource centre, still apply. In no event shall the Royal Society of Chemistry be held responsible for any errors or omissions in this Accepted Manuscript or any consequences arising from the use of any information it contains.

ROYAL SOCIETY OF CHEMISTRY

rsc.li/materials-a

Revealing the beneficial effects of Ge doping on $Cu_2ZnSnSe_4$ thin film solar cells

Markus Neuschitzer[1]*, Moises Espindola Rodriguez[1], Maxim Guc[1], Jose Marquez[2,3], Sergio Giraldo[1], Ian Forbes[2], Alejandro Perez-Rodriguez[1,4], and Edgardo Saucedo[1]

[1] Catalonia Institute for Energy Research- IREC, Jadins de les Dones de Negre 1, 08930 Sant Adrià de Besòs (Barcelona), Spain

[2] Northumbria Photovoltaic Applications Group, Department of Physics and Electrical Engineering, Northumbria University, Newcastle upon Tyne, UK

[3] Department of Structure and Dynamics of Energy Materials, Helmholtz-Zentrum-Berlin, Hahn-Meitner-Platz 1, D-14109 Berlin, Germany

[4] IN2UB, Departament d'Electrònica, Universitat de Barcelona, C. Martí i Franquès 1, 08028 Barcelona, Spain

*E-mail:mneuschitzer@irec.cat

Abstract:

Kesterite (CZTSe) is a promising thin film photovoltaic absorber material due to its composition of more earth abundant materials compared to mature thin film photovoltaic technologies. Up to now, power conversion efficiencies are still lower and its main problem is the low open circuit voltage (V_{oc}). Recently, a novel sintering approach using a nanometric Ge layer showed a large increase in device performance and especially in V_{oc}. In this work, in-depth solar cell characterization as well as Raman and Photoluminescence studies of devices employing different Ge doped CZTSe absorber layers is presented. The main focus is to reveal the beneficial effects of Ge doping and furthermore investigate the interaction of Ge and Na. For low Ge doping an increase in charge carrier concentration is observed, resulting in devices with V_{oc} of 460 mV, which corresponds to V_{oc} deficits ($E_g/q–V_{oc}$) of 596 mV a value comparable to current record devices. For high Ge amounts admittance spectroscopy measurements identified the appearance of a deep defect which can explain the observed deterioration of solar cell performance. Additional Na provided during crystallization of high Ge doped devices can reduce the density of this deep defect and recover device performance. These results indicate that Na plays an important role in defect passivation and we propose a defect model based in the interaction of group IV elements and Na with Cu vacancies.

1. Introduction

Kesterites are quaternary semiconductor compound based on Cu, Zn, Sn, and Se and/or S ($Cu_2ZnSn(S,Se)_4$ - CZTSSe). In recent years, these materials have attracted more and more attention due to the similarity of their properties to the already more established $Cu(In,Ga)Se_2$ (CIGSe) photovoltaic absorbers and a composition free of scare elements like In and Ga. Currently the certified record efficiency of sulphur and selenium containing solid solution $Cu_2ZnSn(S,Se)_4$ based solar cells is 12.6% which is still much lower than efficiencies of CIGSe record devices which recently surpassed 22%.[1], [2] One of the main challenges so far for kesterite solar cells is the low open circuit voltage. The V_{oc} depends on the bandgap of the absorber and can be reduced due to recombination.[3] Therefore, to compare absorbers with different bandgap a so called V_{oc} deficit is introduced, which is defined as $V_{oc-def} = E_g/q - V_{oc}$. Record kesterite devices hardly overcome a V_{oc} deficit of 0.6 V, whereas record CIGSe devices show V_{oc} deficits of below 0.4 V.[1], [2] The reasons for this lack of V_{oc} are currently intensively investigated. Besides the occurrence of detrimental secondary phases different possible explanation were proposed.

Enhanced interface recombination was proposed as one reason.[4]–[7] It could be linked to a cliff like band alignment observed for high bandgap, i.e. sulphur rich kesterite absorbers and the CdS buffer layer.[8], [9] However, for low bandgap, i.e. selenium rich kesterite this is not the case.[9]–[12] For sulphur pure absorbers, V_{oc} losses due to recombination at the interface can be overcome by employing alternative buffer layer different than CdS with better band alignment.[13], [14] Therefore, interface recombination cannot be the main cause for the high V_{oc} loss.

A low minority carrier lifetime was suggested as further reason for V_{oc} loss, however theoretical device simulation shows that low minority carrier lifetime alone does not account for all V_{oc} loss.[7], [15]

Furthermore, the presence of tail states was proposed as a reason for low V_{oc} values.[7], [16], [17] Tail states are a non-zero density of states located at the bandgap edges, which reduces the optical bandgap to a so called mobility gap. Band tails are evidenced by the fact that the maximum of the peak of photoluminescence measurements of kesterite samples is usually noticeable red-shifted compared to the optical bandgap which can be explained by band tails, as band-tail to band-tail transition are observed.[7], [11], [16] Furthermore, a slow decay of the IQE signal below bandgap which is frequently observed in kesterite devices is another indication for sub-bandgap absorption.[7], [18] Electrostatic potential fluctuations or bandgap fluctuations are proposed to be responsible for this non zero density of states within the bandgap.[7] The origins of electrostatic potential fluctuation are charged defects whereas bandgap fluctuations can be explained by local in homogeneities in the absorber layer, like non-uniform composition, ordered/disordered domains or secondary phases.[7], [17] Tail states can be quantified by the Urbach Energy E_u because sub-bandgap absorption can be described by $\alpha \propto \exp\left(-\frac{E_g - E}{E_u}\right)$.[19] De Wolf et al.[20] showed for different photovoltaic materials a linear relationship between Urbach energy and V_{oc} deficit, where lowest E_u resulted in lowest V_{oc} deficit. Cu/Zn disorder in the kesterite lattice was suspected to be responsible for tail states, however recent studies show that up to now no clear correlation between Cu/Zn ordering, tail states, and further V_{oc} deficit could be found and the origins of the large tails are still not totally clear.[11], [17]

Deep defects could be another reason for the reduced V_{oc} values of kesterite solar cells. Larramona et al. showed that by careful control of the Sn content during synthesis, the formation of deep defects related to Sn vacancies/antisites could be avoided and device performance improved.[21] Wei et al. observed a deep donor defect which compensates the CZTSSe absorber and proposed that the deep defect together with a short carrier diffusion length could be responsible for high V_{oc} deficit.[22] Furthermore, trap assisted tunnelling recombination is suggested as possible reason for low voltage.[18], [23]

Recently, a novel sintering approach using a nanometric Ge layer deposited onto metallic precursor stacks or nanocrystalline precursors prior to a reactive annealing in Se and Sn atmosphere showed a large increase in device performance and especially in V_{oc}.[24]–[26] Differently to beneficial Ge alloying in kesterites reported previously [27]–[30] minimal quantities of Ge are observed in the final CZTSe absorber using this Ge nanolayer approach. [24]–[26]

The goal of this work is to get a deeper insight into the beneficial effects of Ge doping on device performance. It is surprising that there is an optimum amount of Ge in the range of 5-15 nm that has to be added during synthesis of either metal stacks or nanocrystalline precursors to improve device performance. Higher Ge amounts added enhance grain growth significantly but are detrimental for cell performance. [24], [25], [31] The purpose of this study is to shed light on the beneficial effects of Ge doping by defect spectroscopy as well as Raman and photoluminescence (PL) measurements. Three different solar cells devices out of a series with different Ge-doping are presented here in detail. The first one was synthesized without Ge addition (0 nm Ge), the second was synthesized with 10 nm Ge evaporated on top of the nanocrystalline precursor before a crystallization step, which corresponds to the range of optimal Ge doping. The third was obtained employing high Ge addition (50 nm Ge) during crystallization step under selenium atmosphere. Furthermore, the strong interaction of Ge and Na is demonstrated by investigating Ge and additionally Na doped absorbers.

2. Experimental details

First Cu/Sn/Cu/Zn metallic stacks deposited by DC magnetron sputtering onto Mo coated soda lime glass were selenized at low temperatures of 350ºC for 30 minutes under Ar flow keeping the pressure at 1.5 mbar to form a nanocrystalline precursor layer. On top of the precursors different thicknesses of Ge or NaF+Ge where thermally evaporated. Then the precursors with

the different capping layers were annealed under selenium atmosphere using a two-step profile, with a first step at 400ºC and Ar flux keeping the pressure at 1.5 mbar for 15 minutes, followed by a high temperature step at 550ºC and 1 bar for 15 minutes. A detailed description of the Ge doping process can be found in [24]. Solar cell devices were finished by depositing CdS buffer and iZnO/ITO window layer as described in more detail in [32]. A post deposition annealing of the complete cell on a hotplate in air at temperature below 250ºC was carried out to improve device performance.[33]

Solar cells were characterized measuring JV curves under illumination of a 100 mW/cm^2 simulated solar spectrum by an Abet technology AAA solar simulator. Temperature dependent JV curves were recorded using a closed cycle He cryostat and an Oriel small area solar simulator calibrated to 1 sun with a Si reference cell.

External quantum efficiency (EQE) measurements were performed using a Bentham PVE300 system calibrated with Si and Ge photodiodes.

CV and Cf measurements at different temperatures (from 100K to 320K) were carried out using a liquid nitrogen cryostat from SemiMetrics Ltd and an Agilent E4980A LCR meter employing a parallel circuit model to extract the capacitance of the device.

Raman scattering (RS) and photoluminescence (PL) spectra were measured using the *i*HR320 Horiba Jobin Yvon spectrometer coupled with CCD and InGaAs detectors. The first detector was used for RS and second for PL spectra. Solid state laser with a 532 nm wavelength was used as excitation source for both methods. Spectra were measured in backscattering configuration through the Olympus metallographic objective and using the maximum laser power which ensured the absence of the thermal effects on the samples. Laser power was changed by changing the current applied for the laser. Sample temperature was varied in the closed-cycleHe cryostat and measured by Si-diode.

3. Results and discussion
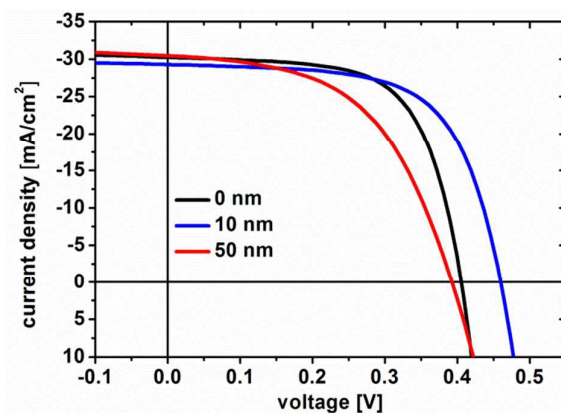
3.1. Electrical and Raman characterization

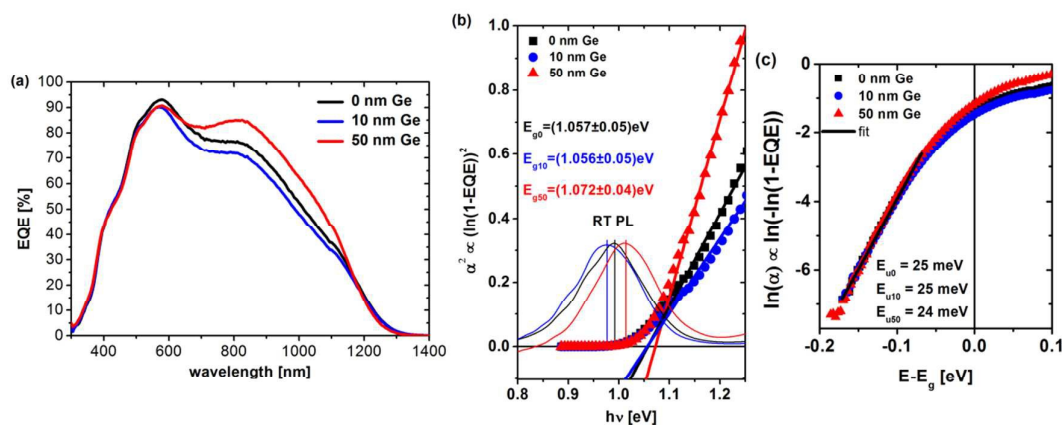**Figure 1. JV curves of solar cells doped with different amount of Ge during absorber synthesis.**

Figure 2. External quantum efficiency (a), bandgap extraction of EQE compared to RT PL (b), and extraction of Urbach energy from ln(-ln(1-EQE)) below the bandgap.

**Table 1. Device parameters of solar cells with different Ge doping. N_{cv} and SCR are extracted at 132 kHz.**

sample	Efficiency [%]	FF [%]	J_{sc} [mA/cm^2]	V_{oc} [mV]	R_{series} [Ω.cm^2]	R_{shunt} [Ω.cm^2]	A	J_0 [mA/cm^2]	E_g [eV]	$E_g/q-V_{oc}$ [V]	N_{cv} [cm^{-3}]	SCR [nm]
0 nm Ge	7.9	64.9	30.2	**405**	0.02	340	1.8	5.1×10^{-3}	1.057	**0.652**	1.8×10^{15}	317
10 nm Ge	8.6	64.1	29.3	**460**	0.27	780	1.9	3.2×10^{-3}	1.056	**0.596**	1.5×10^{16}	114
50 nm Ge	6.3	52.5	30.5	**393**	1.23	272	2.2	7.1×10^{-2}	1.072	**0.679**	6.2×10^{14}	622

In Figure 1 the JV curves of the three devices are shown as well as the device parameters are

listed in Table 1. A clear improvement in V_{oc} is observed for the 10 nm Ge device compared to

the 0 nm Ge reference. For the 50 nm Ge device a decrease in V_{oc} is observed. The bandgap was extracted from quantum efficiency (QE) measurements by assuming collection just in the space charge region (SCR, W), thus QE can be approximated by $QE \cong 1 - exp(-\alpha W)$, where α is the absorption coefficient.[34] The absorption coefficient is proportional to the bandgap of the absorber by[35] $\alpha(h\upsilon) \propto \sqrt{h\upsilon - E_g}$. Thus by plotting $(\ln(1 - QE))^2 \ vs. \ h\upsilon$ and linear fitting of the long wavelength (low energy part) one can get the bandgap as the intercept with the $h\upsilon$-axis (see Figure 2 (b)). The bandgap stays constant around 1.05 eV up to a Ge amount of 10 nm and increases for the 50 nm Ge case. This is expected for higher Ge incorporation in the lattice.[36]

Raman measurements confirm the low Ge incorporation into the CZTSe lattice for Ge amounts up to 10 nm, as is shown in Figure 3. In the 0 nm Ge sample the position of all Raman peaks at room temperature (RT) corresponds to the ones published previously for CZTSe compounds[37] and no peaks of secondary phases were found. The position of the most intense peak for the sample with 0 nm Ge and 10 nm of Ge are similar, whereas the position of this peak in the 50 nm Ge sample shifts about 1 cm^{-1} to the higher wavenumbers. This indicates that in the last sample a $Cu_2ZnSn_xGe_{1-x}Se_4$ solid solution was formed with x ≈ 0.9[37], while in the sample with 10 nm of Ge almost no Ge was incorporated and Ge acts most possibly as a dopant. However, in the sample with 10 nm of Ge a small increase of the asymmetry of the most intense peak comparing to the reference sample was observed. According to Valakh et.al., this is related to an increase of disorder in the samples.[38], [39] With lowering the sample temperature a small blue shift of all Raman peaks was detected, which reached the 2 cm^{-1} at 20 K. Note that the shift was independent on the Ge content which indicates that its inclusion in the lattice do not create any additional strains and the change of lattice tensile with temperature, which is responsible for the shift of Raman peaks, is similar for all the samples.

Journal of Materials Chemistry A Accepted Manuscript
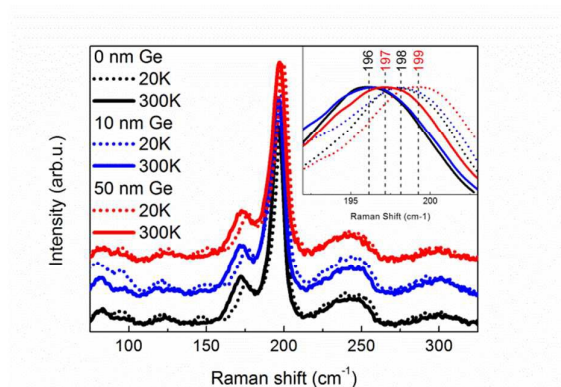
Figure 3. Raman scattering spectra of CZTSe layer with different thickness of Ge layer measured at different temperatures. The inset shows the enlarged region with the most intense peak.

Since the bandgap stays constant up to 10 nm Ge while the V_{oc} increases, the V_{oc} deficit can be reduced to below 600 mV. The increase in V_{oc} can therefore not be related to a bandgap increase due to Ge incorporation into the lattice[36] and has to have different origins as will be discussed in the following. The efficiency follows the same trend. The highest efficiency of 8.6% is obtained for the lowest V_{oc} deficit. In literature band tails were proposed as one of the main performance bottleneck in kesterite based solar cells causing low V_{oc} values.[7], [40] One can characterize band tails which are responsible for sub-bandgap absorption by the Urbach energy E_u. Below the bandgap the absorption coefficient can be approximated by by

$\alpha \propto \exp\left(-\frac{E_g - E}{E_u}\right)$ to extract E_u.[19] In Figure 5.3 (c) $\ln(\alpha) \propto x/E_u \, vs. \, (E - E_g)$ is shown for all devices and E_u extracted by linear fitting. An Urbach energy of around 25 meV is obtained with no significant difference between the different devices. Furthermore, these band tails are responsible for an pronounced red-shift of the main peak of room temperature (RT) photoluminescence (PL) measurements compared to the optical bandgap.[11], [16], [17] For all different Ge doped samples this red-shift is observed as can be seen in Figure 2 (b).Therefore, it can be concluded that Ge doping unfortunately does not modify band tails and reasons for efficiency improvements have to be different.

The diode parameters, like series resistance, diode quality factor and saturation current density extracted following procedure proposed by Sites et al. and Hegedus et al. (see

supporting Information S1) are summarized in Table 1.[34], [41] Diode quality factor for all

three devices is close to 2, where for the 50 nm Ge devices it is slightly higher. This suggest

that the main recombination path is recombination in the space charge region for all three

samples.[42] The saturation current density of the 10 nm Ge devices is the lowest, whereas the

one of the 50 nm Ge samples is one order of magnitude higher indicating an enhanced

recombination as origin for the lower V_{oc} value obtained. To further investigate recombination

mechanism in the devices temperature dependent JV measurements were carried out.
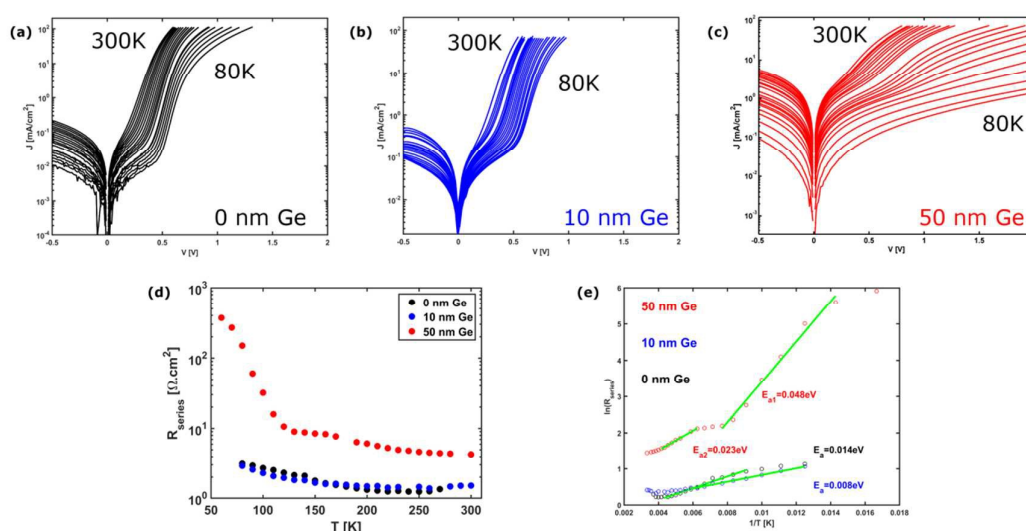
Figure 4. Temperature dependent dark JV curves (a)-(c) and dark series resistance (d) extracted for each temperature and exponential fits to extract activation energies (e).

In Figure 4, temperature dependent dark JV curves of all 3 devices are shown. Remarkable is

the increase in series resistance at low temperature for the 50 nm Ge devices, as can be seen

by the strong downward bending of the JV curves at higher forward bias. An exponential

increase in series resistance is observed, where for the 50 nm Ge device one can distinguish

two regions. The observed temperature dependence indicates a thermal activation of the

carriers, thus the series resistance can be described by $R_s = R_0 \exp(\frac{E_a}{kT})$, where E_a is the

activation energy.[43] In earlier studies this exponential increase in series resistance was

related to an non-ohmic back contact of Kesterite and MoS(e)$_2$/Mo interface[5] however it is

more likely that bulk conductivity itself limits the series resistance.[44] Gunawan et al. related

the exponential increase in series resistance to a carrier freeze out due to the fact that the dominant acceptor defect is quite deep, e.g. 0.13-0.2 eV above the valence band depending on the bandgap of the absorber.[44] In Figure 4 the extraction of the activation energies of the series resistances are shown for all three devices. For the 10 nm device the lowest activation energy of 8 meV was found. For the 0 nm Ge devices it increases to 14 meV, and for the 50 nm Ge device two regions have to be distinguished. For the first temperature range of 300-150 K an activation energy of 23 meV was found which increases to 48 meV for temperatures <130 K. Similar observations of two thermally activated processes are reported in literature, where the first activation energy is related to grain boundaries or shallow acceptor like defects and the second one at lower temperature to different processes like carrier localization in potential wells, radiative recombination or Mott's variable range hopping where holes occupy shallow states in the band gap and if a sufficient high concentration of this states is present the overlapping of their wave functions could form an impurity band.[43], [45] Since the high temperature activation energy is the lowest for the 10 nm Ge device an reduction of grain boundary barrier height for the optimal Ge doping range of 10 nm could be speculated because in this temperature range thermionic emission across grain boundaries is typically the dominant conduction mechanism.[46] However, more detailed conductivity measurements of the thin films itself would be necessary to confirm it.
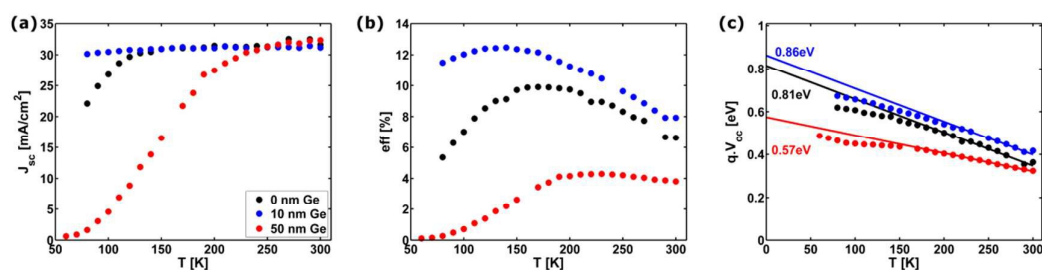

Figure 5. Temperature dependent solar cell device parameters (short circuit current (a) and efficiency (b)) and extraction of V_{oc} to 0K (c).

Besides dark JV-T analysis, the illuminated curves were recorded as well and device parameters extracted, In Figure 5 the J_{sc}, efficiency (eff) as well as V_{oc} for different temperatures is shown. From temperature dependent V_{oc} measurements the activation energy

of the main recombination path can be determined by extrapolating the V_{oc} to 0K.[42] Comparing this value with the bandgap of the absorber could lead to conclude about possible V_{oc} limitations due to the interface, i.e. unfavourable band alignment of absorber and buffer layer.[42] For the 0 nm Ge and 10 nm Ge values of 0.81 eV and 0.86 eV were obtained, respectively. These values are lower than the bandgap extracted from EQE, however since kesterite absorbers suffers from strong band tailing the V_{oc} at 0 K should be compared to the energy of the radiative recombination in the bulk , i.e. to the maximum of the PL spectrum.[16] The values are similar to that of RT PL peaks (see Figure 2(b)) thus for 0 nm Ge and 10 nm Ge device the main recombination is bulk recombination as commonly observed for selenium rich kesterite.[43] Surprisingly the V_{oc} at 0 K for the 50 nm Ge device is much lower, and an activation energy of 0.57 eV is obtained, This could be either related to a non-ideal diode like behaviour like a strong temperature dependent diode factor or voltage dependent carrier collection which makes the extraction of activation energy invalid[47] or a change of band alignment of the Ge containing kesterite with the CdS buffer to a cliff like alignment.

Furthermore, a strong decrease in J_{sc} for the 50 nm Ge device at low temperature is observed which is correlated with the strong increase of series resistance. For the 0 nm Ge device this decrease is less pronounced, and for the 10 nm Ge devices almost no decrease is observed. The efficiency behaves the same way, a strong decrease for the 50 nm and 0 nm Ge device, whereas the 10 nm Ge devices continuously increases until almost 100 K. Quenching of efficiency at low temperature is commonly observed in kesterite devices and related to the carrier freeze out, i.e. strong increase of series resistance.[48] Kim et al. showed that by employing a In_2S_3/CdS double buffer layer, the CZTSSe absorber doping level could be increased by In doping and the low temperature quenching eliminated, as well as the efficiency at room temperature improved.[48] In the following, it will be shown that for the optimum Ge doping range of 10 nm also an increase in doping is observed which could explain that for the 10 nm Ge device no quenching at all is observed.

One interesting feature in the EQE measurements shown in Figure 2 that was not commented yet is the increased EQE signal in the long wavelength region for the 50 nm Ge device, which is in agreement with a higher J_{sc} obtained. Doping profiles derived from CV measurements (see Figure 6) show an increase in charge carrier density for the 10 nm Ge sample followed by a decrease for the 50 nm Ge device. The space charge region (SCR) extracted at 0 V from the profiles shows the highest value for the 50 nm Ge case (see Table 1), which can explain the improved collection in the long wavelength region of the EQE. Assuming a change only in the absorber doping (N) one can estimate the change in V_{oc} by $\Delta V_{OC} = kT/qln(\frac{N_1}{N2})$.[3] The increase in doping of around one order of magnitude from 1.8×10^{15} cm^{-3} to 1.5×10^{16} as it is observed for the 0 nm Ge compared to the 10 nm Ge device would result in a V_{oc} improvement of 55 mV, which corresponds perfectly to the observed V_{oc} improvements. The decrease of doping density for the 50 nm Ge is surprising and might be related to a different mechanism. As already observed in previous work [24] there is high frequency dependence, for the 50 nm Ge device, of the doping profile observed. This is a strong indication for the presence of deep defects.[49]
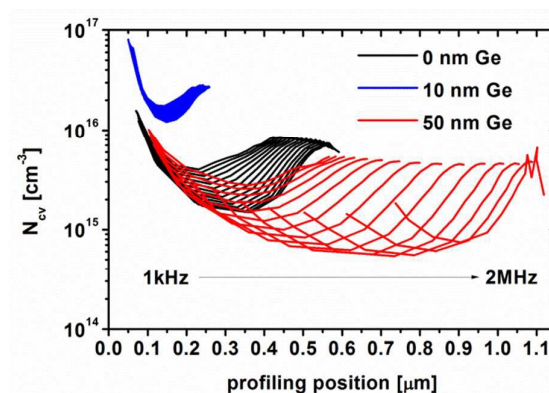

Figure 6. Doping profiles derived from CV measurements at different frequencies.

To further investigate defects in the three devices admittance spectroscopy measurements were carried out as shown in Figure 7. Two capacitance steps are present in the 50 nm Ge device, whereas for the 10 nm Ge device just one step is visible (see Figure 7 (c) and (e)). Similar Cf spectra were obtained for devices presented in previous work[24] confirming the
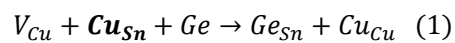
reproducibility of the process and measurements. In the Cf spectrum of the 0 nm Ge reference device also two steps are visible (see Figure 7 (a)). The defect spectra derived from admittance spectroscopy measurements using the method proposed by Walter et al.[50] are shown in Figure 7 (b),(d) and (f). For all cases a shallow defect around 100 mV is observed which gets shallower for the optimal Ge doping of 10 nm. Remarkable is the appearance of a deep defect for the 0 nm Ge as well as the 50 nm Ge device with activation energies above 400 meV. The values of activation energy extracted for this set of sample agree well with the once extracted from a different set investigated in previous work[24] confirming the reproducibility of the processes. Recently Larramona et al. [21] showed that by fine tuning the Sn concentration the formation of a deep defect (600 meV), probably Cu_{Sn} antisites or V_{Cu} formed due to Sn loss, could be avoided and efficiency increased over 11%.
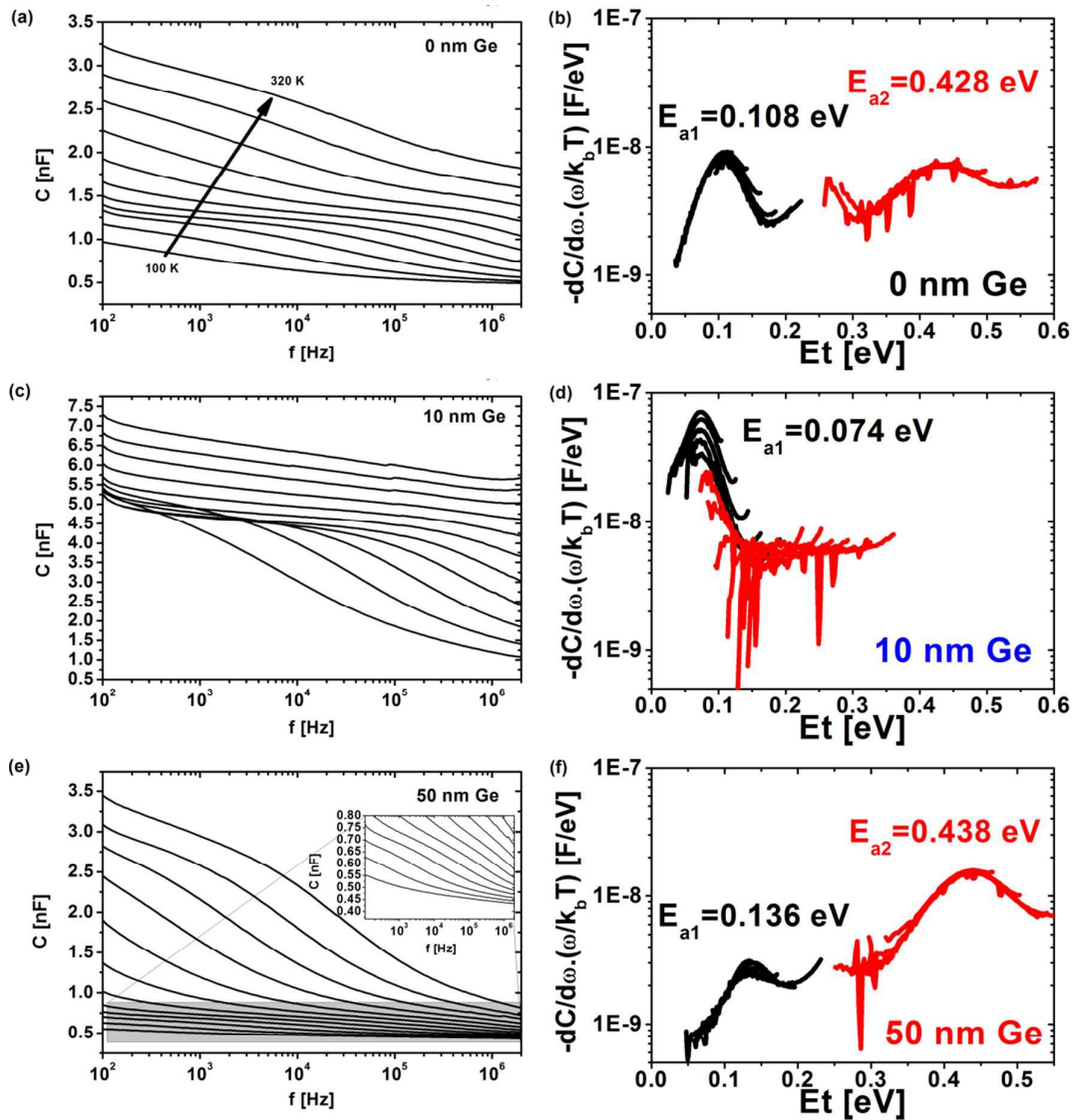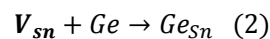
**Figure 7. C-f spectra at different temperature (a),(c),(e) and defect spectra derived from it (b),(d),(f).**

This in in agreement with our observations for 10 nm Ge sample where Ge could compensate

Sn loss and avoid a deep defect formation like Cu_{Sn} or V_{sn} as already proposed in [24]:

$$V_{Cu} + \boldsymbol{Cu_{Sn}} + Ge \rightarrow Ge_{Sn} + Cu_{Cu} \quad (1)$$

or

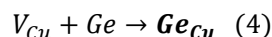$$\boldsymbol{V_{sn}} + Ge \rightarrow Ge_{Sn} \quad (2)$$

Journal of Materials Chemistry A

For high Ge content (i.e. 50 nm Ge) the formation of Cu_{Sn} is less likely because the CZTSe absorber are synthesized as Cu poor and in this case group IV element (Sn,Ge) rich. Thus the formation of Sn_{Cu} or Ge_{Cu} antisites donor defects seems more likely under this growth conditions:

$$V_{Cu} + Sn_{Sn} + Ge \rightarrow Ge_{Sn} + \boldsymbol{Sn_{Cu}} \quad (3)$$

or

$$V_{Cu} + Ge \rightarrow \boldsymbol{Ge_{Cu}} \quad (4)$$
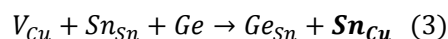
Ge replaces Sn and the excess Sn could lead to the formation of Sn_{Cu} or Ge_{Cu} antisites defects. Sn_{Cu} creates a deep donor defect[51], [52] which acts as electron-hole recombination centre deteriorating the solar cell performance. This would further explain the lower doping observed for high Ge (50 nm) devices due to compensation. Recently Wei et al. [22] showed by admittance spectroscopy measurements and simulations that a deep n-type defect is present in a 10% CZTSSe solar cell, which could be a key limitations of the device performance and was possible assigned to Sn_{Cu} or Sn_{Zn} donor defects which is in line with our observations. For the optimum Ge doping range of 10 nm Ge added during absorber synthesis the formation of deep defects either due to Sn loss or group IV elements antisites defects could be avoided and highest device performance is achieved. Still the reason for increased doping, which might be responsible for the increased V_{oc} besides the reduced recombination, due to the elimination of deep defects and as also evidenced by the lowest saturation current density (see Table 1) is not totally clear. A possible interaction of Na, a well-known dopant in chalcogenide photovoltaic absorbers and Ge could be responsible for it as will be discussed later on in more detail.

3.2. Photoluminescence measurements
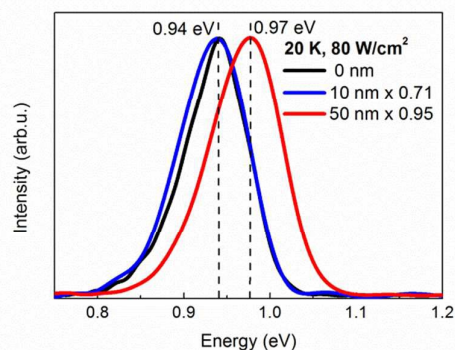
Figure 8. PL spectra of CZTSe layer with different thickness of Ge. The spectra were normalized to the PL intensity of the 0 nm Ge sample and numbers in the legend show the normalization coefficient

To further investigate possible defects which are active in radiative processes photoluminescence (PL) measurements were carried out. Unfortunately due to detector limitations possible PL bands related to midgap defects cannot be assessed. Nevertheless valuable information about recombination processes and shallow defects can be obtained from temperature dependence of PL spectra around the bandgap. In Figure 8, PL spectra of three analyzed samples measured at 20 K with highest excitation power are presented. The maximum peak position is not changed in the sample with 10 nm of Ge comparing to the 0 nm Ge one, while for the sample with 50 nm of Ge a shift to higher energy is observed. This correlates with Raman data which indicated the formation of new phase of $Cu_2ZnSn_xGe_{1-x}Se_4$ solid solution which has higher band gap than the pure CZTSe phase, and is also coherent with the higher band gap observed in EQE data.[36] To determine the nature of the observed PL spectra, an excitation power dependence study of PL spectra in all samples has been performed. Selected spectra of the sample with 10 nm of Ge are presented in Figure 9(a). Analysis of these spectra showed a strong blue shift of the peak maximum with excitation power. The increase is about 18 meV/decade (see Figure 9(b)). Additionally the analysis of the integrated PL intensity versus excitation power showed an exponential dependence in accordance with formulae $I_{PL} \sim I_{ex}{}^k$. The exponent k was found to be lower than 1 (see Figure 9(c)). This indicates the defect related nature of the observed PL spectra, while the strong blue

shift of the maximum is an indication for a quasi-donor-acceptor pair (QDAP) recombination as radiative processes in the analyzed samples.[53] The QDAP recombination was previously found in pure CZTSe[54] and CZTS[55], [56] compounds, as well as in their solid solutions.[54] It is characterized by a strong influence of the band bending due to a fluctuating potential, to the PL band maximum position, which could be described by [53]:

$$E_{PL} = E_g - (E_A + E_D) - 2\Gamma \quad (5)$$

Here E_g is the band gap energy, E_A and E_D are the activation energies of the acceptor and donor, respectively, involved in the irradiative process and coefficient Γ is the average potential wells depth.[53]
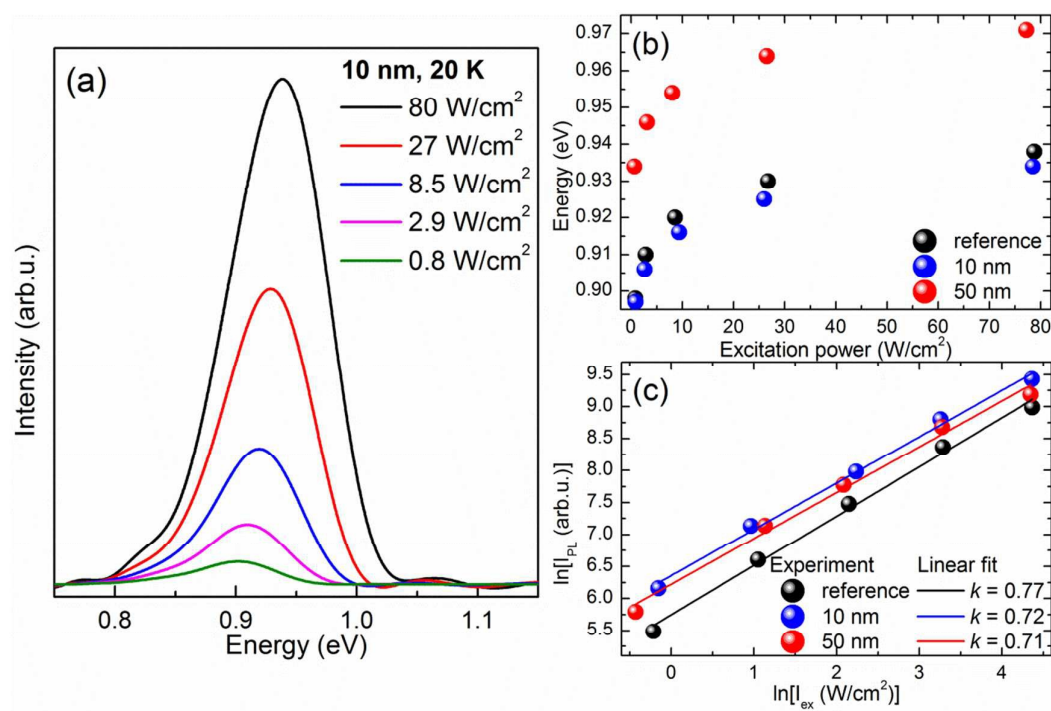
Figure 9. (a) Excitation power dependence of the PL spectra of CZTSe layer with 10 nm of Ge. (b) Maximum peak position vs. excitation power. (c) Integrated PL intensity vs. excitation power.

The analysis of temperature dependence of PL spectra (Figure 10(a)) showed a red shift of the band maximum up to ~ 100 K and a blue shift at higher temperatures (Figure 10(b)). Similar dependencies were observed in case of CZTSSe solid solutions for the QDAP emission[54], [57]. A strong quenching of PL intensity of about 3 orders in the analyzed temperature range 20 −

300 K (Figure 10(c)) was found in the studied samples. This quenching could be described using the equation with two activation energies [58]:

$$I_{PL} = \frac{I_0}{1 + a_1 \exp(-E_1/k_B T) + a_2 \exp(-E_2/k_B T)} \quad (6)$$

where a_1 and a_2 are the rate parameters of the non-irradiative process with activation energies E_1 and E_2. I_0 is PL intensity at lowest temperature and k_B is Boltzmann constant. Both activation energies obtained from fitting of integrated PL intensity are almost constant in the 0 nm and 10 nm Ge samples and increase in case of sample with 50 nm of Ge (see Figure 10(c)). Note that in the framework of QDAP recombination model the lower E_1 energy is attributed to the average value of the valley depth, from which the carriers should be thermally activated for the subsequent recombination, rather than to the activation energy of some shallow defect level.[54] Obtained values of E_1, i.e. the depth valley in the analyzed samples, showed only a slight change with Ge content used in agreement with extracted Urbach energy from EQE for all samples (see Figure 2(c)). However, the E_1 value is smaller than the tails energy for all samples, yielding that potential fluctuations are only one of possible reasons of their formation.

The higher activation energy E_2 could be attributed to a donor or acceptor level involved in the recombination process. At temperatures higher than 250 K the radiative mechanism of the observed PL spectra was found to be changed from QDAP to the band to impurity (BI) recombination, which is proven by the constant maximum position with excitation power change at 300 K. Since the CZTSe absorber has p-type conductivity the transitions acceptor-conduction band is most probable as origin for the observed PL band near room temperature. From the band gap energy found in EQE and the position of PL band maximum at 300 K the activation energy of the involved acceptor level (E_A) was roughly estimated to be in the range 58 – 79 meV for all the samples. This range is in agreement with the energy level found by

admittance spectroscopy. Some discrepancies found for 0 nm and 50 nm Ge device higher could be due to uncertainties of extraction of defect energies when two capacitance steps overlap or the increasing series resistance at low temperatures.[59], [60] Following the logic proposed by Levcenco et al.[54] E_2 energy of 70-118 meV is attributed to a donor defect level (E_D) and a deeper acceptor level should exist in the band gap to ensure the QDAP recombination process.

In summary, from the study of defect levels present in the band gap using admittance spectroscopy and photoluminescence, we obtained two shallow levels at ~ 0.1 eV (one donor and one acceptor) and one deep level at ~ 0.4 eV. The later only exist in 0 nm and 50 nm Ge samples and could be one of the reason of their reduced efficiency comparing to 10 nm Ge device.
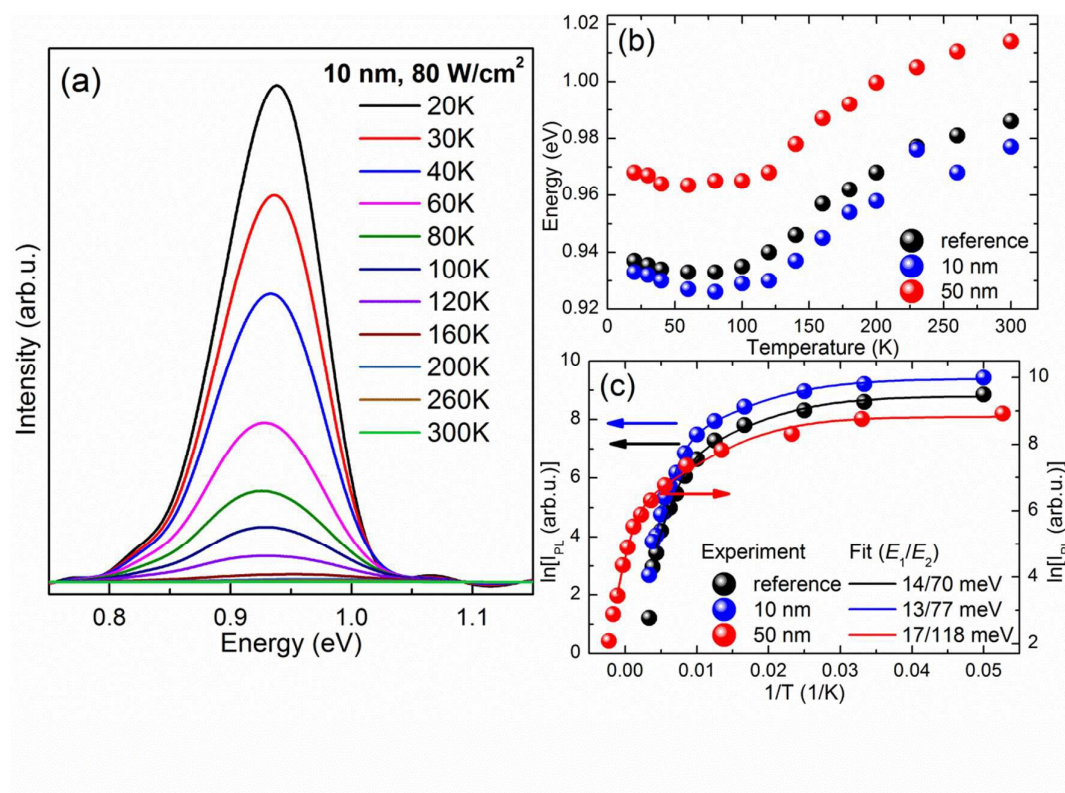
Figure 10. (a) Temperature dependence of the PL spectra of CZTSe layer with 10 nm of Ge. (b) Maximum peak position vs. sample temperature. (c) Integrated PL intensity vs. sample temperature.

3.3. Interaction of Ge and Na

The reasons for the increased charge carrier density for the optimum Ge doping of 10 nm, as observed by CV profiling (see Figure 6) is still not clear yet. Recently our group discovered a possible interaction of Ge and Na, a well-known dopant in kesterite based solar cells.[61] As shown in Giraldo et al. [61] a higher amount of Na was found in the absorber layer synthesized using the optimum range of about 10 nm Ge, whereas higher Ge amounts used during synthesis led to a decrease in Na in the absorber. The Na amount found correlate well with the doping profiles obtained, where as it is shown in this study a higher doping level is obtained for 10 nm Ge devices whereas for higher Ge amounts (>25 nm) a decrease in doping density is observed.[61] In Giraldo et al. NaO_x crystals were found on top of absorbers synthesized under addition of high Ge quantities, thus an extraction of Na from the absorber towards the absorber surface was proposed due to the formation of a GeSe-liquid phases which can dissolve Na in large amounts. Furthermore, element IV (Sn,Ge) rich growth increases the probability of Ge_{Cu} and Sn_{Cu} anitistes and therefore hinder the incorporation of Na due to the fact that Na most likely occupies Cu vacancies (Na_{Cu}).[61], [62] Furthermore, absorbers synthesized on sodium free substrates like Si/SiO_2 showed that Ge assisted synthesis is only beneficial for device performance if additional Na is added by evaporation of a NaF layer.[61] This fact was further confirmed by different Na free substrates like stainless steel.[63] To get more insights in the possible interaction between Na and Ge, a sample series with optimum as well as high Ge range was prepared but with additional Na added by depositing NaF on top of nanocrystalline precursors before Ge deposition. Thermally evaporated NaF on top of precursor layers has been shown already in literature to be an effective source of additional Na during the synthesis of CZTSe absorber layers.[64] Two different thicknesses of NaF (10 nm and 15 nm) where thermally evaporated onto nanocrystalline precursors followed by deposition of a 10 nm and 25 nm Ge capping layer in the same evaporation chamber without breaking the vacuum. Then these nanocrystalline precursors with Ge and NaF+Ge capping layer were annealed under selenium atmosphere as described in the experimental details. In Figure 11,

box plots of the device parameters of the different samples are shown. For the optimum Ge amount of 10 nm, the addition of Na has no significant influence on device performance. However, for the sample synthesized with large Ge amount of 25 nm, additional Na clearly improves device performance especially V_{oc}. To probe if the additional NaF layer may change the Ge incorporation into the film, the bandgap values extracted from EQE (Figure 12(a)) measurements are compared in Figure 12(b) for the 25 nm Ge series. No significant difference is observed, indicating that the additional Na has no influence on Ge incorporation from the point of view of possible bandgap changes.
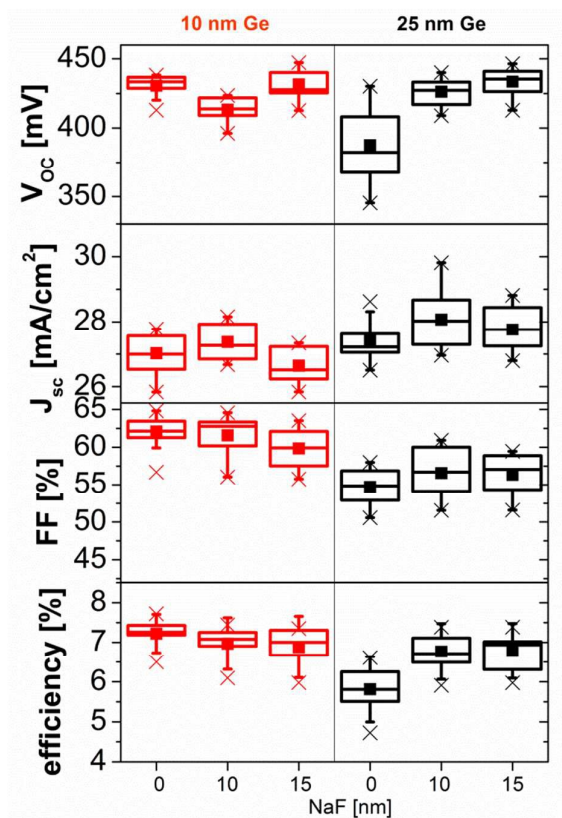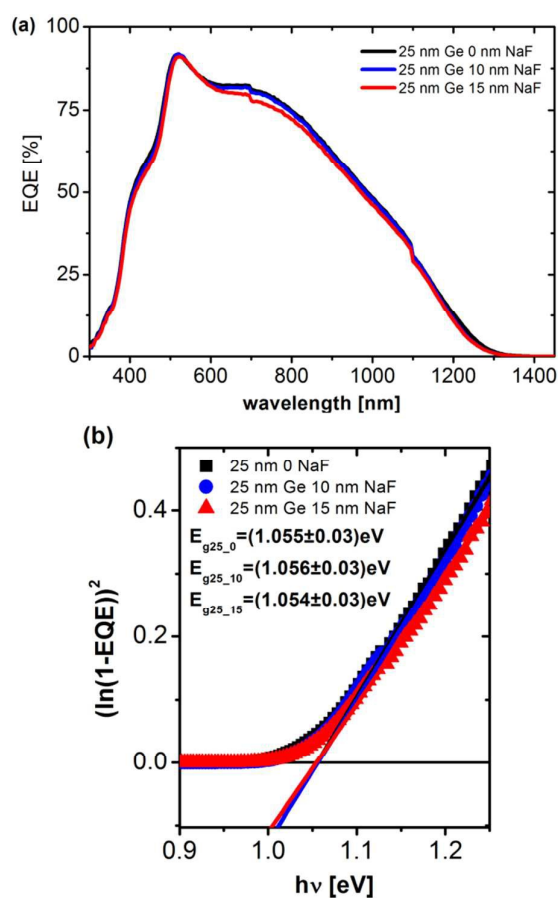

Figure 11. Box plot of device parameters of absorbers synthesized under the addition of Ge and NaF.

Figure 12. EQE as well as bandgap extraction from EQE.

Two different devices are investigated in more detail in the following. One which employs an absorber layer that was synthesized under Ge rich condition by adding 25 nm Ge on top of nanocrystalline precursor prior selenization and one which was synthesized using the same amount of Ge but additionally 15 nm NaF were evaporated on top before Ge evaporation. In Figure 13(a), the JV curve of the best cell of the two devices is shown. A clear improvement in V_{oc} is observed for the Ge+NaF device and device performance could largely be improved as can be seen in Table 2.
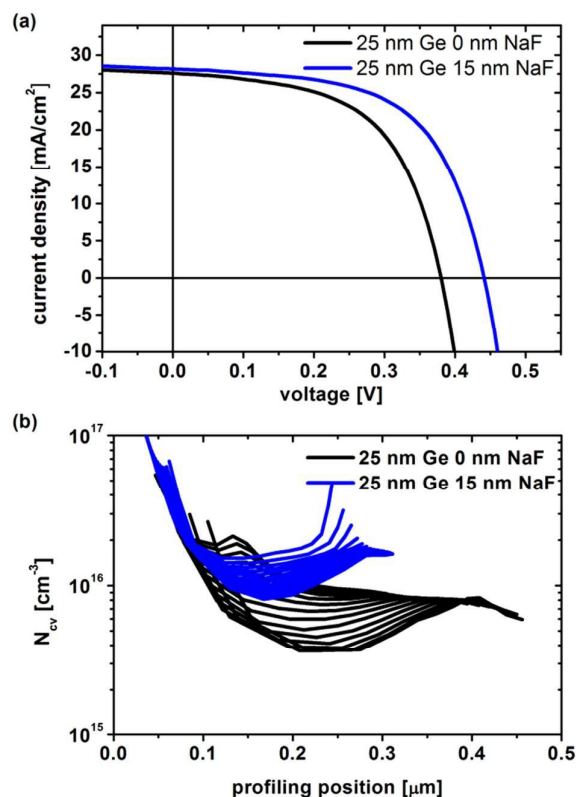
Figure 13. (a) Doping profiles extracted from CV measurements at different frequencies as well as the illuminated JV curves (b) for Ge and Ge+Na doped devices.

Table 2. Device parameters of solar cells with Ge and Ge+Na doping. N_{cv} and SCR are extracted at 132 kHz.

Sample 25 nm Ge	Efficiency [%]	FF [%]	J_{sc} [mA/cm^2]	V_{oc} [mV]	R_{series} [Ω.cm^2]	R_{shunt} [Ω.cm^2]	A	J_0 [mA/cm^2]	E_g [eV]	E_g/q-V_{oc} [V]	N_{cv} [cm^{-3}]	SCR [nm]
+0 nm NaF	6.0	56.7	27.6	**381**	0.04	246	2.3	4.3×10^{-2}	1.055	**0.674**	5.7×10^{15}	161
+15 nm NaF	7.4	59.4	28.2	**441**	0.30	359	2.3	2.2×10^{-2}	1.054	**0.613**	1.1×10^{16}	118

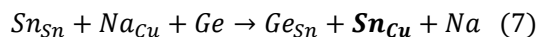Doping profiles extracted from CV measurements of the two devices are shown in Figure 13(b).

An increase in doping density for the Ge+Na device can be observed, as well as the frequency

dependence of the doping profiles could be reduced. Admittance spectroscopy measurements

were carried out as well on the devices as can be seen in Figure 14. In the Cf spectrum of the

device which absorber was synthesized just by 25 nm Ge addition and without additional Na

(Figure 14 (a)), clearly two capacitance steps can be seen as it was observed for all absorbers

synthesized using large amounts of Ge (>25 nm). The defect spectra extracted from the Cf

measurements shows a shallower defect at around 163 meV, which for this device was found

at higher activation energy compared to the devices investigated before (see Figure 14(b) and compare to Figure 7). Additionally, a deep defect at 325 meV was found as it was detected for all devices with absorbers that were synthesized with thick Ge capping layers (>25 nm). Here this deep defect seems less pronounced which could be explained by the fact that less Ge (25 nm instead of 50 nm) was used during synthesis, thus less Ge_{Cu} or Sn_{Cu} antisites are probably formed. In the Cf spectrum of the 25 nm Ge + 15 nm NaF sample the high temperature capacitance step is not obvious anymore and only a step at low temperatures is clearly observed, which activation energy was found to be around 113 meV.
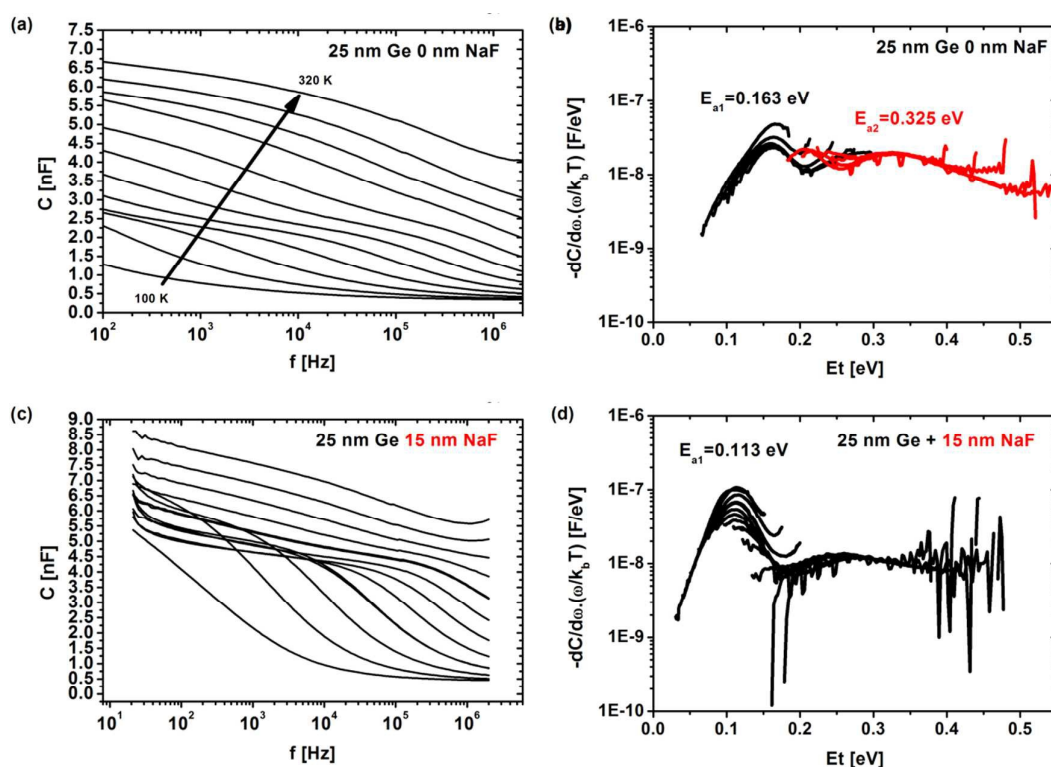
Figure 14. Cf spectra at different temperatures as well as from it derived defect spectra for Ge and Ge+Na doped devices.
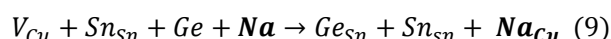
The elimination of the deep defect by controlled Na addition confirms the suspected interaction between Ge and Na. As proposed in Giraldo et al. large amount of Ge used during synthesis, create an element IV (Sn,Ge) rich growth conditions, which could lead to the release of Na out of the absorber.[61] The Ge-Na dynamics for this case can be illustrated by
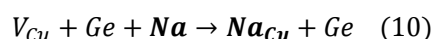
$$Sn_{Sn} + Na_{Cu} + Ge \rightarrow Ge_{Sn} + \boldsymbol{Sn_{Cu}} + Na \quad (7)$$

or

$$Na_{Cu} + Ge \rightarrow \boldsymbol{Ge_{Cu}} + Na \quad (8)$$

Thus, large amounts of Ge supplied during a synthesis could led to the replacement of Na_{Cu}, releasing Na of the absorber and led to the formation of Sn_{Cu} or Ge_{Cu} antisites, which are deep donor defects as discussed earlier and deteriorate cell performance.[51], [52] A sufficient high additionally supply of Na can avoid this process and therefore, no deep defects related to Ge_{Cu} or Sn_{Cu} and higher device performance is observed as could be illustrated by

$$V_{Cu} + Sn_{Sn} + Ge + \boldsymbol{Na} \rightarrow Ge_{Sn} + Sn_{sn} + \boldsymbol{Na_{Cu}} \quad (9)$$

or

$$V_{Cu} + Ge + \boldsymbol{Na} \rightarrow \boldsymbol{Na_{Cu}} + Ge \quad (10)$$

The observed increased doping density for the Ge+NaF device can be explained by the reduced formation of compensating donor defects, and additional due to the expected higher Na amount in the absorber, which is known to increase doping of kesterite absorbers and as also observed here makes acceptor defects shallower.[62], [65] Therefore, for the optimum Ge doping range of around 10 nm Ge, it is reasonable to assume that the right amount of Ge added during synthesis on one hand avoids the formation of V_{Sn} or Cu_{Sn} antisites which could form due to Sn loss, and furthermore moderates the Na amount inside the final absorber layer.

4. Conclusions

A detailed study investigating the beneficial effects of Ge doping on device performance has been presented. For the optimal Ge amount provided during synthesis (i.e. around 10 nm), a large increase in V_{oc} is observed, which can be explained by an increase in doping density as well as a reduction of recombination due to the fact that the formation of deep defects is

avoided as evidenced by admittance spectroscopy. For the device without Ge doping as well as for the one synthesized with the addition of a high Ge amount (50 nm), deep midgap defects have been found as possible reason for lower device performance and especially higher V_{oc} deficit. These defects could potentially be assigned to V_{Sn} or Cu_{Sn} antisites caused due to Sn loss, or Sn_{Cu} or Ge_{Cu} antisites formed due to element IV rich growth conditions. Controlled Ge addition in low quantities could avoid the formation of these defects by compensating possible Sn loss, besides the beneficial effects on grain growth due to the formation of liquid Ge-Se phase as shown in previous work.[24] Furthermore, the quenching of efficiency at low temperatures commonly reported in kesterite devices is not observed for optimal range of Ge doping, thus the device behaviour gets more similar to that of high performance CIGS solar cells.[48]

PL of all three samples shows similar behavior, with QDAP transition at low temperatures and BI transitions at RT. The activation energy of acceptor level involved in the BI transition of 58-79 meV agrees well with the values obtained from admittance spectroscopy of the 10 nm Ge sample and is comparable for the 0 nm and 50 nm Ge samples. From fitting of the temperature dependence of the integrated PL intensity associated to the QDAP transition a donor level between 70-119 meV was found. The activation energy associated with the depth of the valleys, due to potential fluctuations, only changes slightly between the samples as well as band tails observed from EQE measurements suggesting no significant influence of Ge doping to these parameters

Furthermore, a clear interaction of Ge and Na has been demonstrated. Excessive Na addition to samples synthesized under Ge rich condition could avoid the formation of deep defects formed normally under this growth conditions. In summary a careful control of group IV element content (Ge, Sn) is necessary during the growth of kesterite absorbers to avoid the formation of deep defects which are detrimental for the device performance and especially

the V_{oc}. This could be either achieved by controlled Ge doping or by additionally supply of Na,

which as has been demonstrated hinder the formation of detrimental deep defects.

Acknowledgements

[1]   W. Wang *et al.*, "Device characteristics of CZTSSe thin-film solar cells with 12.6% efficiency," *Adv. Energy Mater.*, vol. 4, no. 7, pp. 1–5, 2014.

[2]   P. Jackson, R. Wuerz, D. Hariskos, E. Lotter, W. Witte, and M. Powalla, "Effects of heavy alkali elements in Cu(In,Ga)Se$_2$ solar cells with efficiencies up to 22.6%," *Phys. status solidi - Rapid Res. Lett.*, Aug. 2016.

[3]   U. Rau and H.-W. Schock, "Electronic properties of Cu (In, Ga) Se2 heterojunction solar cells–recent achievements, current understanding, and future challenges," *Appl. Phys. A*, vol. 69, no. 2, pp. 131–147, 1999.

[4]   O. Gunawan, T. K. Todorov, and D. B. Mitzi, "Loss mechanisms in hydrazine-processed Cu[sub 2]ZnSn(Se,S)[sub 4] solar cells," *Appl. Phys. Lett.*, vol. 97, no. 23, p. 233506, 2010.

[5]   D. A. R. Barkhouse, O. Gunawan, T. Gokmen, T. K. Todorov, and D. B. Mitzi, "Device characteristics of a 10.1% hydrazine-processed Cu2ZnSn(Se,S)4 solar cell: Characteristics of a 10.1% efficient kesterite solar cell," *Prog. Photovoltaics Res. Appl.*, vol. 20, no. 1, pp. 6–11, Jan. 2012.

[6]   J. J. Scragg *et al.*, "Rapid annealing of reactively sputtered precursors for Cu$_2$ZnSnS$_4$ solar cells: Rapid annealing of sputtered precursors for Cu$_2$ZnSnS$_4$ solar cells," *Prog. Photovoltaics Res. Appl.*, vol. 22, no. 1, pp. 10–17, Jan. 2014.

[7]   T. Gokmen, O. Gunawan, T. K. Todorov, and D. B. Mitzi, "Band tailing and efficiency limitation in kesterite solar cells," *Appl. Phys. Lett.*, vol. 103, no. 10, 2013.

[8]   M. Bär *et al.*, "Cliff-like conduction band offset and KCN-induced recombination barrier enhancement at the CdS/Cu2ZnSnS4 thin-film solar cell heterojunction," *Appl. Phys. Lett.*, vol. 99, no. 22, pp. 98–101, 2011.

[9]   N. Terada *et al.*, "Characterization of electronic structure of Cu2ZnSn(SxSe1−x)4 absorber layer and CdS/Cu2ZnSn(SxSe1−x)4 interfaces by in-situ photoemission and inverse photoemission spectroscopies," *Thin Solid Films*, vol. 582, pp. 166–170, 2015.

[10]   G. Brammertz *et al.*, "Characterization of defects in 9.7% efficient Cu2ZnSnSe4-CdS-ZnO solar cells," *Appl. Phys. Lett.*, vol. 103, no. 16, p. 163904, Oct. 2013.

[11]   G. Rey *et al.*, "Ordering kesterite improves solar cells: A low temperature post-deposition annealing study," *Sol. Energy Mater. Sol. Cells*, vol. 151, pp. 131–138, 2016.

[12]   R. Haight *et al.*, "Band alignment at the Cu₂ZnSn(S[sub x]Se[sub 1−x])[sub 4]/CdS interface," *Appl. Phys. Lett.*, vol. 98, no. 25, p. 253502, 2011.

[13]   C. Platzer-Björkman *et al.*, "Reduced interface recombination in Cu2ZnSnS4 solar cells with atomic layer deposition Zn1-xSnxOy buffer layers," *Appl. Phys. Lett.*, vol. 107, no. 24, pp. 1–5, 2015.
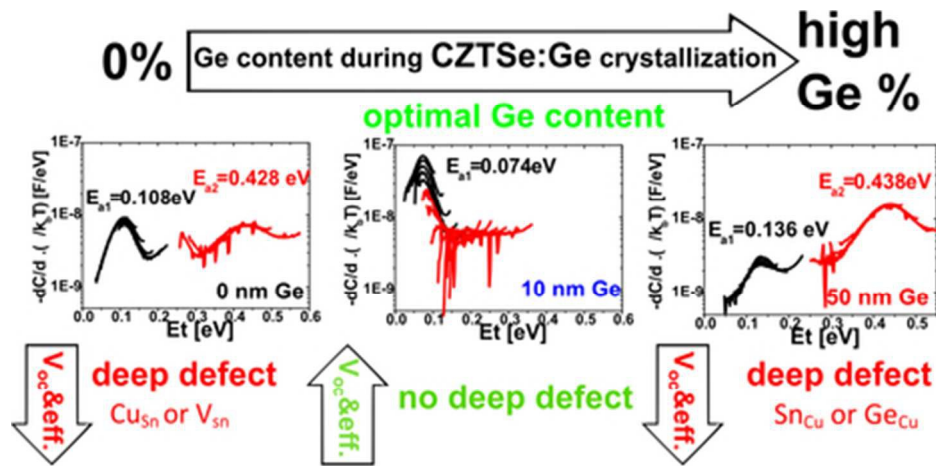
[14]   K. Sun *et al.*, "Over 9% Efficient Kesterite Cu $_2$ ZnSnS $_4$ Solar Cell Fabricated by Using Zn $_{1-}$
$_x$ Cd $_x$ S Buffer Layer," *Adv. Energy Mater.*, Apr. 2016.

[15]   I. L. Repins *et al.*, "Indications of short minority-carrier lifetime in kesterite solar cells,"
J. Appl. Phys., vol. 114, no. 8, 2013.

[16]   S. Siebentritt *et al.*, "What is the bandgap of kesterite?," *Sol. Energy Mater. Sol. Cells*,
vol. 158, pp. 126–129, 2016.

[17]   S. Bourdais *et al.*, "Is the Cu/Zn Disorder the Main Culprit for the Voltage Deficit in
Kesterite Solar Cells?," *Adv. Energy Mater.*, vol. 6, no. 12, pp. 1–21, 2016.

[18]   C. J. Hages, N. J. Carter, and R. Agrawal, "Generalized quantum efficiency analysis for
non-ideal solar cells: Case of Cu2ZnSnSe4," *J. Appl. Phys.*, vol. 119, no. 1, 2016.

[19]   F. Urbach, "The Long-Wavelength Edge of Photographic Sensitivity and of the Electronic
Absorption of Solids," *Phys. Rev.*, vol. 92, no. 5, pp. 1324–1324, Dec. 1953.

[20]   S. De Wolf *et al.*, "Organometallic Halide Perovskites: Sharp Optical Absorption Edge
and Its Relation to Photovoltaic Performance," *J. Phys. Chem. Lett.*, vol. 5, no. 6, pp.
1035–1039, Mar. 2014.

[21]   G. Larramona *et al.*, "Fine-Tuning the Sn Content in CZTSSe Thin Films to Achieve 10.8%
Solar Cell Efficiency from Spray-Deposited Water-Ethanol-Based Colloidal Inks," *Adv.
Energy Mater.*, vol. 5, no. 24, 2015.

[22]   S.-Y. Wei *et al.*, "Achieving high efficiency Cu2ZnSn(S,Se)4 solar cells by non-toxic
aqueous ink: Defect analysis and electrical modeling," *Nano Energy*, vol. 26, pp. 74–82,
Aug. 2016.

[23]   M. Courel, F. A. Pulgarín-Agudelo, J. A. Andrade-Arvizu, and O. Vigil-Galán, "Open-
circuit voltage enhancement in CdS/Cu2ZnSnSe4-based thin film solar cells: A metal–
insulator–semiconductor (MIS) performance," *Sol. Energy Mater. Sol. Cells*, vol. 149, pp.
204–212, May 2016.

[24]   M. Neuschitzer *et al.*, "V $_{oc}$ Boosting and Grain Growth Enhancing Ge-Doping Strategy
for Cu $_2$ ZnSnSe $_4$ Photovoltaic Absorbers," *J. Phys. Chem. C*, Apr. 2016.

[25]   S. Giraldo *et al.*, "Large Efficiency Improvement in Cu2ZnSnSe4 Solar Cells by
Introducing a Superficial Ge Nanolayer," *Adv. Energy Mater.*, vol. 5, no. 21, 2015.

[26]   S. Giraldo *et al.*, "How small amounts of Ge modify the formation pathways and
crystallization of kesterites," *Energy Environ. Sci.*, pp. 0–29, 2017.

[27]   S. Bag, O. Gunawan, T. Gokmen, Y. Zhu, and D. B. Mitzi, "Hydrazine-processed Ge-
substituted CZTSe solar cells," *Chem. Mater.*, vol. 24, no. 23, pp. 4588–4593, 2012.

[28]   C. J. Hages *et al.*, "Improved performance of Ge-alloyed CZTGeSSe thin-film solar cells
through control of elemental losses: Improved performance of CZTGeSSe solar cells,"
Prog. Photovoltaics Res. Appl., vol. 23, no. 3, pp. 376–384, Mar. 2015.

[29]   S. Kim, K. M. Kim, H. Tampo, H. Shibata, and S. Niki, "Improvement of voltage deficit of
Ge-incorporated kesterite solar cell with 12.3% conversion efficiency," *Appl. Phys.
Express*, vol. 9, no. 10, pp. 1–5, 2016.

[30]   A. D. Collord and H. W. Hillhouse, "Germanium Alloyed Kesterite Solar Cells with Low
Voltage Deficits," *Chem. Mater.*, vol. 28, no. 7, pp. 2067–2073, 2016.

[31]   S. Giraldo *et al.*, "Cu $_2$ ZnSnSe $_4$ solar cells with 10.6% efficiency through innovative
absorber engineering with Ge superficial nanolayer: Cu $_2$ ZnSnSe $_4$ solar cells with 10.6%
efficiency," *Prog. Photovoltaics Res. Appl.*, 2016.

[32]   M. Neuschitzer *et al.*, "Optimization of CdS buffer layer for high-performance Cu$_2$
ZnSnSe$_4$ solar cells and the effects of light soaking: elimination of crossover and red
kink: CdS and effects of light soaking: elimination of crossover and red kink," *Prog.
Photovoltaics Res. Appl.*, vol. 23, no. 11, pp. 1660–1667, Nov. 2015.

[33]   M. Neuschitzer *et al.*, "Complex Surface Chemistry of Kesterites: Cu/Zn Reordering after
Low Temperature Postdeposition Annealing and Its Role in High Performance Devices,"
Chem. Mater., vol. 27, no. 15, pp. 5279–5287, 2015.

[34]   S. S. Hegedus and W. N. Shafarman, "Thin-film solar cells: device measurements and

analysis," *Prog. Photovoltaics Res. Appl.*, vol. 12, no. 23, pp. 155–176, 2004.

[35] J. I. Pankove, *Optical processes in semiconductors*, Unabridged. Mineola [NY]: Dover, 1975.

[36] M. Grossberg, K. Timmo, T. Raadik, E. Kärber, V. Mikli, and J. Krustok, "Study of structural and optoelectronic properties of Cu2Zn(Sn1–xGex)Se4 (x=0 to 1) alloy compounds," *Thin Solid Films*, vol. 582, pp. 176–179, May 2015.

[37] M. Guc, S. Levcenko, V. Izquierdo-Roca, X. Fontané, E. Arushanov, and A. Pérez-Rodríguez, "Polarized Raman scattering analysis of Cu2ZnSnSe4 and Cu2ZnGeSe4 single crystals," *J. Appl. Phys.*, vol. 114, no. 19, 2013.

[38] M. Y. Valakh *et al.*, "Raman scattering and disorder effect in Cu $_2$ ZnSnS $_4$," *Phys. status solidi - Rapid Res. Lett.*, vol. 7, no. 4, pp. 258–261, Apr. 2013.

[39] R. Caballero *et al.*, "Non-stoichiometry effect and disorder in Cu2ZnSnS4 thin films obtained by flash evaporation: Raman scattering investigation," *Acta Mater.*, vol. 65, pp. 412–417, 2014.

[40] T. Gokmen, O. Gunawan, and D. B. Mitzi, "Semi-empirical device model for Cu2ZnSn(S,Se)4 solar cells," *Appl. Phys. Lett.*, vol. 105, no. 3, pp. 5–10, 2014.

[41] J. R. Sites and P. H. Mauk, "Diode quality factor determination for thin-film solar cells," *Sol. Cells*, vol. 27, no. 1–4, pp. 411–417, 1989.

[42] R. Scheer and H. W. Schock, *Chalcogenide photovoltaics physics, technologies, and thin film devices*. Weinheim; Chichester: Wiley-VCH ; John Wiley [distributor], 2011.

[43] E. Kask, J. Krustok, S. Giraldo, M. Neuschitzer, S. López-Marino, and E. Saucedo, "Temperature dependent electrical characterization of thin film Cu $_2$ ZnSnSe $_4$ solar cells," *J. Phys. D. Appl. Phys.*, vol. 49, no. 8, p. 85101, 2016.

[44] O. Gunawan *et al.*, "Electronic properties of the Cu 2ZnSn(Se,S) 4 absorber layer in solar cells as revealed by admittance spectroscopy and related methods," *Appl. Phys. Lett.*, vol. 100, no. 25, 2012.

[45] N. F. Mott, "Impurity Band Conduction. Experiment and Theorythe Metal-Insulator Transition in an Impurity Band," *Le J. Phys. Colloq.*, vol. 37, no. C4, pp. C4-301-C4-306, 1976.

[46] V. Kosyak, M. A. Karmarkar, and M. A. Scarpulla, "Temperature dependent conductivity of polycrystalline Cu2ZnSnS4 thin films," *Appl. Phys. Lett.*, vol. 100, no. 26, p. 263903, 2012.

[47] C. J. Hages, N. J. Carter, R. Agrawal, and T. Unold, "Generalized current-voltage analysis and efficiency limitations in non-ideal solar cells: Case of Cu2ZnSn(SxSe1–x)4 and Cu2Zn(SnyGe1–y)(SxSe1–x)4," *J. Appl. Phys.*, vol. 115, no. 23, p. 234504, Jun. 2014.

[48] J. Kim *et al.*, "High Efficiency Cu $_2$ ZnSn(S,Se) $_4$ Solar Cells by Applying a Double In $_2$ S $_3$ /CdS Emitter," *Adv. Mater.*, p. n/a-n/a, Aug. 2014.

[49] U. Rau, D. Abou-Ras, and T. Kirchartz, *Advanced characterization techniques for thin film solar cells*. Weinheim, Germany: Wiley-VCH, 2011.

[50] T. Walter, R. Herberholz, C. Müller, and H. W. Schock, "Determination of defect distributions from admittance measurements and application to Cu(In,Ga)Se2 based heterojunctions," *J. Appl. Phys.*, vol. 80, no. 8, p. 4411, 1996.

[51] S. Chen, A. Walsh, X.-G. Gong, and S.-H. Wei, "Classification of Lattice Defects in the Kesterite Cu $_2$ ZnSnS $_4$ and Cu $_2$ ZnSnSe $_4$ Earth-Abundant Solar Cell Absorbers," *Adv. Mater.*, vol. 25, no. 11, pp. 1522–1539, Mar. 2013.

[52] Y. S. Yee, B. Magyari-Köpe, Y. Nishi, S. F. Bent, and B. M. Clemens, "Deep recombination centers in C u2ZnSnS e4 revealed by screened-exchange hybrid density functional theory," *Phys. Rev. B - Condens. Matter Mater. Phys.*, vol. 92, no. 19, pp. 1–13, 2015.

[53] P. W. Yu, "Excitation-dependent emission in Mg-, Be-, Cd-, and Zn-implanted GaAs," *J. Appl. Phys.*, vol. 48, no. 12, pp. 5043–5051, 1977.

[54] S. Levcenko *et al.*, "Deep Defects in Cu 2 ZnSn (S , Se) 4 Solar Cells with Varying Se Content," *Phys. Rev. Appl.*, vol. 5, no. 2, p. 24004, 2016.

[55] T. Gershon, B. Shin, T. Gokmen, S. Lu, N. Bojarczuk, and S. Guha, "Relationship between Cu2ZnSnS4 quasi donor-acceptor pair density and solar cell efficiency," *Appl. Phys. Lett.*, vol. 103, no. 19, pp. 2012–2015, 2013.

[56] T. Gershon, B. Shin, N. Bojarczuk, T. Gokmen, S. Lu, and S. Guha, "Photoluminescence characterization of a high-efficiency Cu2ZnSnS4 device," *J. Appl. Phys.*, vol. 114, no. 15, p. 154905, 2013.

[57] X. Lin *et al.*, "Defect study of Cu2ZnSn(SxSe1-x)4 thin film absorbers using photoluminescence and modulated surface photovoltage spectroscopy," *Appl. Phys. Lett.*, vol. 106, no. 1, 2015.

[58] F. Luckert *et al.*, "Optical properties of high quality Cu2ZnSnSe4 thin films," *Appl. Phys. Lett.*, vol. 99, no. 6, p. 62104, 2011.

[59] T. P. Weiss, A. Redinger, D. Regesch, M. Mousel, and S. Siebentritt, "Direct Evaluation of Defect Distributions From Admittance Spectroscopy," *IEEE J. Photovoltaics*, vol. 4, no. 6, pp. 1665–1670, Nov. 2014.

[60] T. Paul Weiss, A. Redinger, J. Luckas, M. Mousel, and S. Siebentritt, "Admittance spectroscopy in kesterite solar cells: Defect signal or circuit response," *Appl. Phys. Lett.*, vol. 102, no. 20, 2013.

[61] S. Giraldo, M. Neuschitzer, M. Placidi, P. Pistor, A. Perez-Rodriguez, and E. Saucedo, "Cu2ZnSnSe4-Based Solar Cells with Efficiency Exceeding 10% by Adding a Superficial Ge Nanolayer: The Interaction between Ge and Na," *IEEE J. Photovoltaics*, vol. 6, no. 3, pp. 754–759, 2016.

[62] Z.-K. Yuan *et al.*, "Na-Diffusion Enhanced p-type Conductivity in Cu(In,Ga)Se$_2$: A New Mechanism for Efficient Doping in Semiconductors," *Adv. Energy Mater.*, p. 1601191, Aug. 2016.

[63] S. López-Marino *et al.*, "Alkali doping strategies for flexible and light-weight Cu$_2$ZnSnSe$_4$ solar cells," *J. Mater. Chem. A*, vol. 4, no. 5, pp. 1895–1907, 2016.

[64] C. M. Sutter-Fella *et al.*, "Sodium Assisted Sintering of Chalcogenides and Its Application to Solution Processed Cu$_2$ZnSn(S,Se)$_4$ Thin Film Solar Cells," *Chem. Mater.*, vol. 26, no. 3, pp. 1420–1425, 2014.

[65] J. V. Li, D. Kuciauskas, M. R. Young, and I. L. Repins, "Effects of sodium incorporation in Co-evaporated Cu2ZnSnSe4 thin-film solar cells," *Appl. Phys. Lett.*, vol. 102, no. 16, p. 163905, 2013.

Journal of Materials Chemistry A Accepted Manuscript

The beneficial effect of Ge doping on kesterite absorbers is revealed and insights in kesterite´s
intrinsic defect chemistry are given.

39x19mm (300 x 300 DPI)